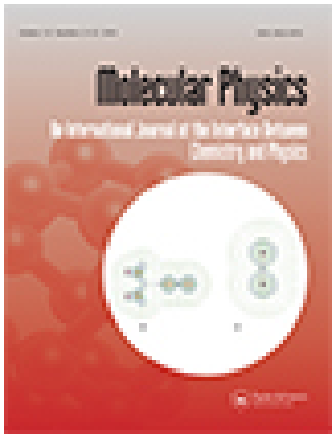

Molecular Physics: An International Journal at the Interface Between Chemistry and Physics

Publication details, including instructions for authors and subscription information:
http://www.tandfonline.com/loi/tmph20

Modelling rotations, vibrations, and rovibrational couplings in astructural molecules - a case study based on the H^+_5 molecular ion

János Sarka[ab], Csaba Fábri[c], Tamás Szidarovszky[bd], Attila G. Császár[ab], Zhou Lin[e] & Anne B. McCoy[e]

[a] Laboratory of Molecular Structure and Dynamics, Institute of Chemistry, Eötvös University, Budapest, Hungary

[b] MTA-ELTE Complex Chemical Systems Research Group, Budapest, Hungary

[c] Laboratory of Physical Chemistry, ETH Zürich, Zürich, Switzerland

[d] Department of Chemistry, School of Science, The University of Tokyo, Tokyo, Japan

[e] Department of Chemistry and Biochemistry, The Ohio State University, Columbus, OH, USA

Published online: 18 Mar 2015.

To cite this article: János Sarka, Csaba Fábri, Tamás Szidarovszky, Attila G. Császár, Zhou Lin & Anne B. McCoy (2015): Modelling rotations, vibrations, and rovibrational couplings in astructural molecules - a case study based on the H^+_5 molecular ion, Molecular Physics: An International Journal at the Interface Between Chemistry and Physics, DOI: 10.1080/00268976.2015.1020074

To link to this article: http://dx.doi.org/10.1080/00268976.2015.1020074

Molecular Physics, 2015
http://dx.doi.org/10.1080/00268976.2015.1020074

SPECIAL ISSUE IN HONOUR OF NICHOLAS C. HANDY

Modelling rotations, vibrations, and rovibrational couplings in astructural molecules – a case study based on the H_5^+ molecular ion

János Sarka[a,b], Csaba Fábri[c], Tamás Szidarovszky[b,d], Attila G. Császár[a,b,*], Zhou Lin[e] and Anne B. McCoy[e]

[a]*Laboratory of Molecular Structure and Dynamics, Institute of Chemistry, Eötvös University, Budapest, Hungary;* [b]*MTA-ELTE Complex Chemical Systems Research Group, Budapest, Hungary;* [c]*Laboratory of Physical Chemistry, ETH Zürich, Zürich, Switzerland;* [d]*Department of Chemistry, School of Science, The University of Tokyo, Tokyo, Japan;* [e]*Department of Chemistry and Biochemistry, The Ohio State University, Columbus, OH, USA*

(*Received 22 December 2014; accepted 12 February 2015*)

One-dimensional (1D) and two-dimensional (2D) models are investigated, which help to understand the unusual rovibrational energy-level structure of the astronomically relevant and chemically interesting astructural molecular ion H_5^+. Due to the very low hindering barrier characterising the 1D torsion-only vibrational model of H_5^+, this model yields strongly divergent energy levels. The results obtained using a realistic model for the torsion potential, including the computed (near) degeneracies, can be rationalised in terms of the model with no barrier. Coupling of the torsional motion with a single rotational degree of freedom is also investigated in detail. It is shown how the embedding-dependent rovibrational models yield energy levels that can be rationalised via the 2D vibrational model containing two independent torsions. Insight into the complex rovibrational energy level structure of the models and of H_5^+ is gained via variational nuclear motion and diffusion Monte Carlo computations and by the analysis of the wavefunctions they provide. The modelling results describing the transition from the zero barrier limit to the large barrier limit should prove to be useful for the important class of molecules and molecular ions that contain two weakly coupled internal rotors.

Keywords: variational nuclear motion theory; reduced-dimensional models; coupling of rotation and vibration; weakly coupled internal rotors; astructural molecules; tunneling; H_5^+

1. Introduction

The simplest and exactly solvable quantum chemical models that are traditionally employed to understand high-resolution spectra of gas-phase molecules are based on the harmonic oscillator (HO) and rigid rotor (RR) approximations of the vibrations and the rotations, respectively. In cases when the results based on the RRHO approximation, perhaps after a slight extension based on second-order perturbation theory [1–5], provide a good qualitative and even a semiquantitative understanding of spectral regularities, the molecule of interest can be considered to be 'semirigid'. These are molecules for which the electronic state that is being investigated contains a single, well-defined, and relatively deep minimum. For semirigid molecules, the timescales for the vibrational and rotational motions are sufficiently different to allow their approximate separation, the vibrational spacing decreases as the vibrational excitation increases, the vibrational states have well-defined symmetries provided by the point group characterising the unique equilibrium structure, and the rotational states can be assigned to a certain vibrational state. The RRHO treatment is familiar to most chemists as excellent textbooks exist which describe slightly anharmonic molecular vibrations [6,7] as well as slow molecular rotations [8]. Nevertheless, there are many molecules and higher energy spectral regions where this simple picture is insufficient for understanding the measured high-resolution spectra.

Nicholas C. Handy was among the pioneers in the area of study developing variational techniques to solve the nuclear Schrödinger equation and thus allowing the community to move far beyond the RRHO approximation [9–14]. Furthermore, his studies of internal coordinate kinetic energy operators [15], some performed with one of the authors [16,17], opened the door to the studies of a broad array of molecules that explore regions of the potential energy surface (PES) where the RRHO approximation begins to break down. There is a special class of molecules where the simple RRHO picture as well as its low-order PT corrections [1] provide an incorrect zeroth-order description and one must consider new models with 'unusual' characteristics to understand the high-resolution spectra of these molecules even at very low excitation energies. We call these molecules astructural [18].

For an astructural molecule, consideration of a single minimum on the PES is insufficient to interpret the observed spectra, when the structure is averaged over the vibrational

* Corresponding author. Email: csaszar@chem.elte.hu

ground state, it is significantly different from the equilibrium Born–Oppenheimer one, rotational and vibrational spacings are of the same magnitude, the usual simple tools provided by the RRHO approximation are unable to yield a reasonable estimate of even the lowest rotational and rovibrational energy levels, and simple perturbative treatments based on the RRHO approximation fail already for the lowest nuclear motion states. Studies of such complex, astructural systems require alternative zero-order pictures to the separable RRHO treatment that has been demonstrated to be effective for semirigid molecules. Often these more sophisticated models involve explicit couplings between the rotation and one or more of the large-amplitude vibrational motions. Considerable attention has been placed in developing such model Hamiltonians for molecules like methanol, that include a large-amplitude internal rotor [19–21], as well as for molecules that contain virtually no barrier to internal rotation [22,23]. As to the spectra of these molecules, the small barriers lead to rotation/vibration structure that deviates substantially from the RRHO model and from those used to describe semirigid molecules, and to very surprising rotational structures [18,24,25].

An example of such an astructural molecule, and one which recently attracted considerable experimental and theoretical attention [18,26–31], is H_5^+. This molecular ion with five hydrogen atoms lacks the usual central atom that can form multiple strong bonds, which is typical of virtually all other small molecular species. Unlike the semirigid molecules, this lack of structure makes the spectrum of H_5^+ particularly challenging to anticipate and interpret. As is usually done for semirigid molecules or for molecules with a single large amplitude motion, to obtain an improved understanding of the rovibrational energy level structure of the astructural H_5^+ molecule, low (one- and two-) dimensional model Hamiltonians must be developed by freezing the remaining rotational-vibrational degrees of freedom (dof). These reduced-dimensional Hamiltonians replace the full-dimensional (12D) rovibrational Hamiltonian and are used to provide physical insight into the motions of the atoms of H_5^+. The vibrational and rovibrational levels of H_5^+ have been computed both by variational nuclear motion [29,30,32,33] and diffusion Monte Carlo (DMC) [31,34,35] techniques. The full- and reduced-dimensional variational computations performed by three of the present authors [18] utilised the GENIUSH algorithm and code [36–38].

In the present contribution, we explore the rotation/torsion coupling in this astrochemically important molecule, focusing on reduced-dimensional models. Such an analysis provides insights into the expected rotational energy progressions. It also lays the foundation for interpreting the results of full-dimensional treatments. While the focus of this paper is on H_5^+, similar 'astructural' behaviour is seen in any molecule or molecular ion in which the barrier to internal rotation is small. These species include, for example, the $NH_4^+ \cdot H_2O$ complex, which was recently studied experimentally by Lee and co-workers [25], and dimethyl acetylene, which is a molecule of long-standing interest [22,23]. The models also provide limiting behaviours on which one can model the spectroscopy of species with slightly larger torsion barriers.

2. Coordinates and embeddings

Using the internal coordinate set, see Figure 1, applied previously [18], two embeddings that differ in the definition of the *xz* plane can be defined for the H_5^+ molecule as follows: either one of the H_2 units can be constrained to lie along the *xz* plane and the other H_2 unit is rotated from that plane by ϕ degrees, or the *xz* plane is defined to bisect ϕ and the two H_2 units are rotated by $\frac{\phi}{2}$ degrees in opposite directions (Figure 2). We shall call the first and the second choices the geometric (GE) and the bisector (BE) embeddings, respectively.

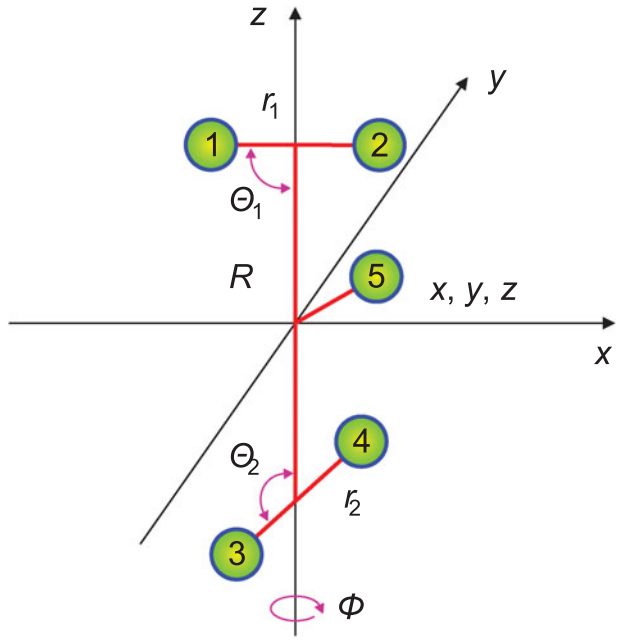

Figure 1. Internal coordinates of H_5^+ employed in this study.

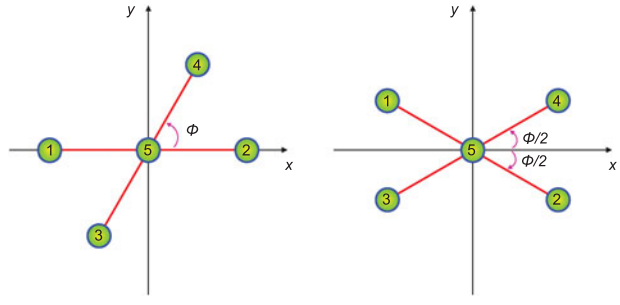

Figure 2. The difference between the geometric, GE, (left panel) and bisector, BE, (right panel) embeddings, viewed from the positive *z* direction.

3. Rovibrational coupling

Although the form of the rotational-vibrational Hamiltonian depends on the applied set of coordinates and the embedding of the molecule-fixed coordinate system, the rovibrational energy levels resulting from a full-dimensional variational solution based on the Hamiltonian must be coordinate and embedding independent. Nevertheless, convergence of the eigenstates toward the 'exact' solution during a variational treatment may depend appreciably on the coordinates, the embedding, and the basis set. To obtain converged rotational-vibrational energy levels, it is desirable to test the chosen set of coordinates, the different embeddings, and the basis sets. Since the rovibrational **G** matrix [6,15] determines the kinetic energy operator, studying the elements of the **G** matrix provides important insight into the differences between distinct internal coordinate and body-fixed embedding choices.

Extremely low potential barriers along the torsional coordinates on the PESs of molecules can result in effectively barrierless motions. Coupling between the different rotational-vibrational dofs has a considerable influence on the rovibrational energy levels. The rovibrational coupling accompanied with the almost free torsion has a direct effect on the rovibrational energy level structure. The astructural H_5^+ molecule is a prototypical example for strong torsional-rotational coupling. In this study, we show the effect of the torsional-rotational coupling on the rovibrational energy level structure of H_5^+ utilising several 1D and 2D model Hamiltonians.

To construct the required reduced- and full-dimensional rovibrational Hamiltonians, one needs to derive first the **G** matrix elements in the GE and BE embeddings. The nuclear position vectors in the geometric embedding, using the nine internal coordinates of Figure 1, are

$$\begin{aligned}
\mathbf{r}_1^{\mathrm{GE}} &= \left(-\frac{r_1}{2}\sin\theta_1, 0, -\frac{r_1}{2}\cos\theta_1 + \frac{R}{2}\right),\\
\mathbf{r}_2^{\mathrm{GE}} &= \left(\frac{r_1}{2}\sin\theta_1, 0, \frac{r_1}{2}\cos\theta_1 + \frac{R}{2}\right),\\
\mathbf{r}_3^{\mathrm{GE}} &= \left(-\frac{r_2}{2}\sin\theta_2\cos\phi, -\frac{r_2}{2}\sin\theta_2\sin\phi, \frac{r_2}{2}\cos\theta_2 - \frac{R}{2}\right),\\
\mathbf{r}_4^{\mathrm{GE}} &= \left(\frac{r_2}{2}\sin\theta_2\cos\phi, \frac{r_2}{2}\sin\theta_2\sin\phi, -\frac{r_2}{2}\cos\theta_2 - \frac{R}{2}\right),\\
\mathbf{r}_5^{\mathrm{GE}} &= (x, y, z). \qquad (1)
\end{aligned}$$

In the bisector embedding, the nuclear position vectors are defined as

$$\begin{aligned}
\mathbf{r}_1^{\mathrm{BE}} &= \left(-\frac{r_1}{2}\sin\theta_1\cos\frac{\phi}{2}, \frac{r_1}{2}\sin\theta_1\sin\frac{\phi}{2}, -\frac{r_1}{2}\cos\theta_1 + \frac{R}{2}\right),\\
\mathbf{r}_2^{\mathrm{BE}} &= \left(\frac{r_1}{2}\sin\theta_1\cos\frac{\phi}{2}, -\frac{r_1}{2}\sin\theta_1\sin\frac{\phi}{2}, \frac{r_1}{2}\cos\theta_1 + \frac{R}{2}\right),\\
\mathbf{r}_3^{\mathrm{BE}} &= \left(-\frac{r_2}{2}\sin\theta_2\cos\frac{\phi}{2}, -\frac{r_2}{2}\sin\theta_2\sin\frac{\phi}{2}, \frac{r_2}{2}\cos\theta_2 - \frac{R}{2}\right),\\
\mathbf{r}_4^{\mathrm{BE}} &= \left(\frac{r_2}{2}\sin\theta_2\cos\frac{\phi}{2}, \frac{r_2}{2}\sin\theta_2\sin\frac{\phi}{2}, -\frac{r_2}{2}\cos\theta_2 - \frac{R}{2}\right),\\
\mathbf{r}_5^{\mathrm{BE}} &= (x, y, z). \qquad (2)
\end{aligned}$$

Note that neither the GE nor the BE Cartesian position vectors given above are defined with respect to the centre of mass (COM) of the H_5^+ molecular ion.

To move toward the desired reduced-dimensional models, we set $x = y = z = 0$ in Figure 1. This places the hydrogen numbered 5 in Figures 1 and 2 at the origin, which is now the COM of H_5^+. We further freeze all of the vibrational dofs except for ϕ, using the values of these coordinates that correspond to the D_{2d} structure, which is a first-order saddle point on the PES of H_5^+ [39]. As such, $r_1 = r_2 = r$, $R = R_0$, and $\theta_1 = \theta_2 = \frac{\pi}{2}$. Note that some rotational matrix elements of the four-dimensional (4D) torsion-rotation **G** matrix were found to depend on the value of ϕ. In case of these matrix elements, we have approximated the ϕ-dependent expressions with their values at $\phi = \pi/2$ (an excellent approximation in the present case, see Ref. [18] for a more detailed discussion). The resulting 4D **G** matrix, corresponding to the torsional vibrational dof (first row and column) plus three rotational dofs (the rest of the rows and columns), can be derived using the position vectors in the geometric embedding which is given by

$$\mathbf{G}^{\mathrm{GE,4D}} = \begin{pmatrix}
\frac{4}{m_{\mathrm{H}}r^2} & 0 & 0 & -\frac{2}{m_{\mathrm{H}}r^2}\\
0 & \frac{2}{m_{\mathrm{H}}(r^2+2R_0^2)} & 0 & 0\\
0 & 0 & \frac{2}{m_{\mathrm{H}}(r^2+2R_0^2)} & 0\\
-\frac{2}{m_{\mathrm{H}}r^2} & 0 & 0 & \frac{2}{m_{\mathrm{H}}r^2}
\end{pmatrix}, \qquad (3)$$

and in the bisector embedding

$$\mathbf{G}^{\mathrm{BE,4D}} = \begin{pmatrix}
\frac{4}{m_{\mathrm{H}}r^2} & 0 & 0 & 0\\
0 & \frac{2}{m_{\mathrm{H}}(r^2+2R_0^2)} & 0 & 0\\
0 & 0 & \frac{2}{m_{\mathrm{H}}(r^2+2R_0^2)} & 0\\
0 & 0 & 0 & \frac{1}{m_{\mathrm{H}}r^2}
\end{pmatrix}. \qquad (4)$$

In these expressions, m_{H} is the mass of the H atom. To obtain the numerical values of the matrix elements $r = 1.4966$ bohr, $R_0 = 4.0977$ bohr, $m_{\mathrm{H}} = 1.007825$ u are used.

Comparing the two $\mathbf{G}^{4D}$ matrices, Equations (3) and (4), one can observe that the only off-diagonal elements are the $G_{14} = G_{41}$ terms in the GE case. These are the only nonzero rovibrational coupling terms in either the GE or

the BE Hamiltonian. These terms are not evident when the bisector embedding is used, reflecting the more balanced treatment of the H_2 rotors in this case.

4. Model Hamiltonians

Although the derived **G** matrix elements are valid for the molecular ion H_5^+, the reduced-dimensional model Hamiltonians to be derived are of relevance for a larger class of molecules where a large-amplitude torsional motion and consideration of rotations are important. First, a 1D vibrational model will be investigated, followed by several 2D extensions.

4.1. The 1D(ϕ) vibrational model

Taking only the torsional motion (ϕ) between the two H_2 units of H_5^+ into account (see Figure 1), a 1D vibrational model Hamiltonian can be obtained

$$\hat{H}^{1D} = -2b_{H_2}\frac{\partial^2}{\partial\phi^2} + \hat{V}(\phi), \tag{5}$$

where the second-derivative operator is multiplied by the constant from the $\mathbf{G}^{4D}$ matrix, $-\frac{1}{2}G_{11}$, and

$$b_{H_2} = \frac{1}{m_H r^2} \tag{6}$$

is the rotational constant of one of the H_2 groups. Since the G_{11} elements in the GE and BE embeddings are equal (see Equations (3) and (4)), the energy levels corresponding to $\hat{H}^{1D}$ are identical, as required. The potential in Equation (5) can be taken as a 1D cut of the full-dimensional PES [28] along the ϕ coordinate, which can be approximated by the function

$$V(\phi) = \frac{V_0}{2}[\cos(2\phi) + 1] + V_{min}, \tag{7}$$

where $V_0 = 80.0894\ cm^{-1}$ and $V_{min} = 197.798\ cm^{-1}$.

As a first task, we solve the eigenvalue problem without the potential energy operator ($V_0 = V_{min} = 0$) analytically by recognising that functions of the form $\exp(ik\phi)$ (k is an integer) are eigenfunctions of the kinetic energy operator. This results in nondegenerate (for $k = 0$) and doubly degenerate (for $k \neq 0$) energy levels (see the $V = 0$ column of Table 1 for the numerical results, corresponding to $b_{H_2} = 53.34\ cm^{-1}$). This observation can easily be explained as follows. The eigenvalues are

$$E_k^{1D} = 2b_{H_2}k^2, \tag{8}$$

where k is any integer (negative, positive, or 0). Clearly, the torsional states diverge rapidly due to the k^2 dependence. Consequently, and unusually for those trained on slightly anharmonic (stretching) motions, H_5^+ might exhibit, depending on the potential, only a few torsional states up to its first dissociation limit.

Table 1. Energies, in cm^{-1}, corresponding to the 1D vibrational model of Equation (5) and employing 21 exponential discrete variable representation (DVR) basis functions for the torsional coordinate (k is defined in Equation (8)).

$\lvert k\rvert$	$V = 0$	$V \neq 0$
0	0.00	(235.97)[a]
1	106.67	88.06
	106.67	128.09
2	426.70	428.25
	426.70	430.13
3	960.06	962.16
	960.06	962.18
4	1706.78	1708.78
	1706.78	1708.78
5	2666.84	2668.79
	2666.84	2668.79
6	3840.26	3842.18
	3840.26	3842.18

[a]This is the zero-point vibrational energy of the model, it was subtracted from the $V \neq 0$ eigenvalues to arrive at the $|k| \neq 0$ energy values reported, thus making them comparable to the $V = 0$ results.

Adding the potential to the equation and using an exponential discrete variable representation (DVR) basis, the kinetic energy matrix elements can be computed analytically, while the potential energy matrix is diagonal in a DVR basis. As a result of adding the potential, the first doublet at 106.7 cm^{-1} splits by 40.0 cm^{-1}, with a slightly increased mean value of 108.1 cm^{-1}. The rest of the eigenvalues change only slightly and the splitting is diminishing as the excitation increases (for $|k| = 2$, 3, and 4, the splittings are 1.88, 0.02, and 0.00 cm^{-1}, respectively, see Table 1). This is an important modelling result as it suggests that there are indeed only a small number of torsional states (only up to $|k| = 4$ or perhaps 5) below the first dissociation limit of H_5^+, about 2500 cm^{-1}. Interestingly, despite the introduction of an 80 cm^{-1} torsion barrier, only the $|k| = 1$ states show significant deviations from the values obtained in the barrierless ($V = 0$) model. The general question how the torsional splittings depend, in the case of the 1D(ϕ) model, on the height of the barrier has been addressed before, see, for example, Refs. [24,40].

4.2. The 2D(ϕ_1, ϕ_2) model

A 2D extension of the 1D(ϕ) Hamiltonian of the previous subsection is defined as

$$\hat{H}^{2D} = -b_{H_2}\left(\frac{\partial^2}{\partial\phi_1^2} + \frac{\partial^2}{\partial\phi_2^2}\right) + \hat{V}(\phi_2 - \phi_1), \tag{9}$$

where the two torsional coordinates are $\phi_1 \in [0, 2\pi]$ and $\phi_2 \in [0, 2\pi]$, and the $\hat{V}$ potential energy operator, coupling the ϕ_1 and ϕ_2 coordinates, depends on only the difference between ϕ_2 and ϕ_1. Setting $\hat{V}$ to zero leads to an uncoupled Hamiltonian for which the eigenproblem can be solved analytically, the energy levels $E^{2D}_{k_1,k_2}$ and wavefunctions $\Psi^{2D}_{k_1,k_2}(\phi_1, \phi_2)$ are

$$E^{2D}_{k_1,k_2} = b_{H_2}(k_1^2 + k_2^2), \tag{10}$$

and

$$\Psi^{2D}_{k_1,k_2}(\phi_1, \phi_2) = \frac{1}{2\pi} \exp(ik_1\phi_1) \exp(ik_2\phi_2). \tag{11}$$

Two important remarks are in order here: (1) the wavefunctions are periodic with a period of 2π in both ϕ_1 and ϕ_2; (2) this periodicity implies that k_1 and k_2 must take integer values. Note that the $\Psi^{2D}_{k_1,k_2}(\phi_1, \phi_2)$ uncoupled eigenstates can be employed for the expansion of the eigenstates of $\hat{H}^{2D}$ (corresponding to a Fourier-series expansion).

As $\hat{V}$ depends only on $\phi_2 - \phi_1$, $\hat{H}^{2D}$ is invariant under an arbitrary rotation of H_5^+ about the z axis. Thus, the projection of the overall angular momentum on z (the corresponding operator is denoted by $\hat{L}$) is conserved and the eigenstates of $\hat{H}^{2D}$ are also eigenstates of $\hat{L}$, and can be labelled by the angular momentum quantum number $L \in \mathbb{Z}$:

$$\hat{L}\Psi^{2D}_{i,L}(\phi_1, \phi_2) = L\Psi^{2D}_{i,L}(\phi_1, \phi_2), \tag{12}$$

where i labels different eigenstates having the same value of $|L|$ in order of increasing energy. Variational results corresponding to the 2D(ϕ_1, ϕ_2) model are presented in Table 2 for the $V = 0$ and $V \neq 0$ cases. Even though L is a good quantum number, in the case of the 2D(ϕ_1, ϕ_2) model the $\Psi^{2D}_{i,L}(\phi_1, \phi_2)$ eigenstates with different values of the L quantum number are not automatically separated. The computed eigenenergies show clear one, two, and fourfold and occasionally nearly eightfold degeneracies in the $V \neq 0$ case (Table 2). These near degeneracies are fully explained by the $V = 0$ results as without the hindering torsional potential the eigenvalues have perfect four and eightfold degeneracies, as expected from Equation (10).

In the subsequent subsections, we present two possible coordinate embedding choices while defining one rotational and one vibrational dof. As a result, the Hamiltonian matrix blocks corresponding to different L values are separated and eigenstates with different L values can be obtained independently.

4.3. The 2D(ϕ, α_{GE}) GE rovibrational model

The first coordinate transformation is defined by the following equations:

$$\begin{aligned} \phi &= \phi_2 - \phi_1, \\ \alpha_{GE} &= \phi_1, \end{aligned} \tag{13}$$

Table 2. Energies, up to 2600 cm^{-1}, corresponding to the 2D(ϕ_1,ϕ_2) model employing 21 exponential DVR basis functions for both torsional coordinates. The eigenenergies of the 2D(ϕ, α_{GE}) and 2D(ϕ, α_{BE}) models are identical with those reported herein. The energies are given in cm^{-1}, $V(\phi)$ is given in Equation (7), and $\Delta E = E(V \neq 0) - E(V = 0)$. The energy values are labelled by $|L|$, an angular momentum quantum number, i, counting the different eigenstates corresponding to the same $|L|$, and $|K_{GE}|$ and $|K_{BE}|$, the torsional quantum numbers in the 2D(ϕ, α_{GE}) and 2D(ϕ, α_{BE}) models, respectively. The degeneracy factor d corresponds to the $V \neq 0$ case; thus, the true $V = 0$ degeneracies can be higher than the $V \neq 0$ ones reported.

$\|L\|$	i	$\|K_{GE}\|$[a]	$\|K_{BE}\|$	d	$E(V=0)$	$E(V\neq 0)$	ΔE
0	1	0	0	1	0.00	235.97	
1	1	(0,1)	1/2	4	53.34	52.72	−0.61
0	2	1	1	1	106.67	88.06	−18.61
2	1	1	0	2	106.67	106.67	0.00
0	3	1	1	1	106.67	128.09	21.42
2	2	(0–2)	1	2	213.35	194.74	−18.61
2	3	(0–2)	1	2	213.35	234.76	21.42
3	1	(1,2)	1/2	4	266.68	266.07	−0.61
1	2	(1,2)	3/2	4	266.68	270.04	3.36
4	1	2	0	2	426.70	426.70	0.00
0	4	2	2	1	426.70	428.25	1.55
0	5	2	2	1	426.70	430.13	3.43
3	2	(0,3)	3/2	4	480.03	483.39	3.36
4	2	(1–3)	1	2	533.37	514.76	−18.61
2	4	(1–3)	2	2	533.37	534.93	1.56
2	5	(1–3)	2	2	533.37	536.80	3.43
4	3	(1–3)	1	2	533.37	554.78	21.42
5	1	(2,3)	1/2	4	693.38	692.77	−0.61
1	3	(2,3)	5/2	4	693.38	695.61	2.23
4	4	(0–4)	2	2	853.39	854.95	1.56
4	5	(0–4)	2	2	853.39	856.82	3.43
3	3	(1,4)	5/2	4	906.73	908.96	2.23
5	2	(1,4)	3/2	4	906.73	910.08	3.36
6	1	3	0	2	960.06	960.06	0.00
0	6	3	3	1	960.06	962.16	2.10
0	7	3	3	1	960.06	962.18	2.12
6	2	(2–4)	1	2	1066.74	1048.13	−18.61
2	6	(2–4)	3	2	1066.74	1068.83	2.10
2	7	(2–4)	3	2	1066.74	1068.86	2.12
6	3	(2–4)	1	2	1066.74	1088.15	21.42
7	1	(3,4)	1/2	4	1333.42	1332.81	−0.61
1	4	(3,4)	7/2	4	1333.42	1335.46	2.04
5	3	(0,5)	5/2	4	1333.42	1335.65	2.23
6	4	(1–5)	2	2	1386.76	1388.32	1.56
4	6	(1–5)	3	2	1386.76	1388.86	2.10
4	7	(1–5)	3	2	1386.76	1388.88	2.12
6	5	(1–5)	2	2	1386.76	1390.19	3.43
3	4	(2,5)	7/2	4	1546.77	1548.81	2.04
7	2	(2,5)	3/2	4	1546.77	1550.12	3.36
8	1	4	0	2	1706.78	1706.78	0.00
0	8	4	4	1	1706.78	1708.78	2.00
0	9	4	4	1	1706.78	1708.78	2.00
8	2	(3–5)	1	2	1813.45	1794.85	−18.61
2	8	(3–5)	4	2	1813.45	1815.45	2.00

(*continued*).

Table 2. (*Continued*)

$\|L\|$	i	$\|K_{GE}\|$[a]	$\|K_{BE}\|$	d	$E(V=0)$	$E(V\neq 0)$	ΔE
2	9	(3–5)	4	2	1813.45	1815.45	2.00
8	3	(3–5)	1	2	1813.45	1834.87	21.42
6	6	(0–6)	3	2	1920.13	1922.22	2.10
6	7	(0–6)	3	2	1920.13	1922.25	2.12
5	4	(1,6)	7/2	4	1973.47	1975.50	2.03
7	3	(1,6)	5/2	4	1973.47	1975.70	2.23
8	4	(2–6)	2	2	2133.48	2135.03	1.55
4	8	(2–6)	4	2	2133.48	2135.47	1.99
4	9	(2–6)	4	2	2133.48	2135.47	1.99
8	5	(2–6)	2	2	2133.48	2136.91	3.43
9	1	(4,5)	1/2	4	2186.81	2186.20	−0.61
1	5	(4,5)	9/2	4	2186.81	2188.78	1.97
3	5	(3,6)	9/2	4	2400.16	2402.13	1.97
9	2	(3,6)	3/2	4	2400.16	2403.51	3.35

[a] For odd $|L|$, two of the fourfold degenerate energy levels with the same $|L|$ can be labelled by one $|K_{GE}|$ quantum number (x) and two by another one (y). Such cases are marked as (x,y). For even $|L|$, where $|L|\neq 0$ and $i>1$, two, twofold degenerate energy levels with the same $|L|$ and $V=0$ energy but different x and y $|K_{GE}|$ quantum numbers are mixed in the $V\neq 0$ case. Such cases are marked as ($x-y$).

where ϕ and α_{GE} describe the relative torsional motion of the two diatoms and the overall rotation of the two diatoms about the z axis, respectively. The transformed Hamiltonian becomes

$$\hat{H}^{2D,GE} = -b_{H_2}\left(2\frac{\partial^2}{\partial\phi^2}+\frac{\partial^2}{\partial\alpha_{GE}^2}-2\frac{\partial^2}{\partial\phi\partial\alpha_{GE}}\right)+\hat{V}(\phi)$$
$$= -b_{H_2}\left(2\frac{\partial^2}{\partial\phi^2}-\hat{L}^2-2i\frac{\partial}{\partial\phi}\hat{L}\right)+\hat{V}(\phi), \quad (14)$$

where the third term couples the vibrational and rotational dofs and $\hat{L}=-i\frac{\partial}{\partial\alpha_{GE}}$. The form of $\hat{H}^{2D,GE}$ is also justified by the matrix elements of $\mathbf{G}^{GE,4D}$ (see Equation (3)).

The next step is to represent the periodic $\hat{V}(\phi)$ potential by a Fourier series:

$$\hat{V}(\phi)=\sum_k V_k\exp(ik\phi), \quad (15)$$

and examine matrix elements of $\hat{H}^{2D}$ expressed in the orthonormal $\Psi^{2D}_{k_1,k_2}(\phi_1,\phi_2)$ uncoupled basis. These integrals can be transformed from the (ϕ_1,ϕ_2) to the (ϕ,α_{GE}) coordinate system

$$\mathbf{H}^{2D}_{k_1,k_2;k_1',k_2'} = \frac{1}{4\pi^2}\int_0^{2\pi}d\phi_1\int_0^{2\pi}d\phi_2\exp(-ik_1\phi_1)$$
$$\times\exp(-ik_2\phi_2)\hat{H}^{2D}\exp(ik_1'\phi_1)\exp(ik_2'\phi_2)$$
$$=\frac{1}{4\pi^2}\int_0^{2\pi}d\alpha_{GE}\int_{-\alpha_{GE}}^{2\pi-\alpha_{GE}}d\phi\exp(-i(k_1+k_2)\alpha_{GE})$$
$$\times\exp(-ik_2\phi)\hat{H}^{2D,GE}\exp(i(k_1'+k_2')\alpha_{GE})\exp(ik_2'\phi)$$
$$=\delta_{LL'}\left[b_{H_2}(2K_{GE}^2+L^2-2K_{GE}L)\delta_{K_{GE}K_{GE}'}+V_{K_{GE}-K_{GE}'}\right]$$
$$=\mathbf{H}^{2D,GE}_{K_{GE},L;K_{GE}',L'}, \quad (16)$$

where the new quantum numbers $K_{GE}=k_2$ and $L=k_1+k_2$ have been introduced and the transformed basis functions are

$$f^{GE}_{K_{GE},L}(\phi,\alpha_{GE})=\frac{1}{2\pi}\exp(iK_{GE}\phi)\exp(iL\alpha_{GE}), \quad (17)$$

with integer K_{GE} and L values, the latter corresponding to the angular momentum quantum number. In this particular case, matrix elements of the potential energy operator defined by Equation (7) take the following form:

$$\mathbf{V}_{K_{GE},L;K_{GE}',L'}=\delta_{LL'}V_{K_{GE}-K_{GE}'}$$
$$=\delta_{LL'}\left[\left(\frac{V_0}{2}+V_{min}\right)\delta_{K_{GE},K_{GE}'}+\frac{V_0}{4}\delta_{2,K_{GE}-K_{GE}'}\right.$$
$$\left.+\frac{V_0}{4}\delta_{2,K_{GE}'-K_{GE}}\right]. \quad (18)$$

It is worth pointing out the following: (1) the $\mathbf{H}^{2D,GE}$ blocks with different L values are not coupled; and (2) the α_{GE}-dependent lower and upper integration limits of ϕ can be modified to 0 and 2π for arbitrary ϕ-dependent periodic basis functions with a period of 2π as the value of the integral does not depend on α_{GE}. The latter statement for matrix elements of an arbitrary 2π periodic operator $\hat{A}(\phi)$ can be proven by Fourier expansion of $\hat{A}(\phi)$ and the periodic ϕ-dependent basis functions $[g_i(\phi)=g_i(\phi+k2\pi), k\in\mathbb{Z}]$

$$\int_{-\alpha_{GE}}^{2\pi-\alpha_{GE}}d\phi g_i^*(\phi)\hat{A}(\phi)g_j(\phi)$$
$$=\sum_{klm}g_{ik}^*A_l g_{jm}\int_{-\alpha_{GE}}^{2\pi-\alpha_{GE}}d\phi\exp[i(l+m-k)\phi]$$
$$=2\pi\sum_{lm}g_{i,l+m}^*A_l g_{jm}. \quad (19)$$

Thus, periodic exponential DVR basis functions can be employed to provide an alternative representation of $\hat{H}^{2D,GE}$:

$$\mathbf{H}^{2D,GE}_{k,L;k',L'}=\frac{1}{2\pi}\int_0^{2\pi}d\alpha_{GE}\int_0^{2\pi}d\phi\exp(-iL\alpha_{GE})f_k^*(\phi)$$
$$\times\hat{H}^{2D,GE}\exp(iL'\alpha_{GE})f_{k'}(\phi)$$
$$=\delta_{LL'}\left[-b_{H_2}\left(2\int_0^{2\pi}d\phi f_k^*(\phi)\left(\frac{\partial^2}{\partial\phi^2}-iL\frac{\partial}{\partial\phi}\right)\right.\right.$$
$$\left.\left.\times f_{k'}(\phi)-L^2\delta_{kk'}\right)+\hat{V}(\phi_k)\delta_{kk'}\right], \quad (20)$$

where $f_k(\phi)$ stands for the kth exponential DVR basis function and ϕ_k is the grid point associated with $f_k(\phi)$. This

vibrational basis was employed in a previous study [18] published on H_5^+ by three of the authors of this paper.

The numerical variational results obtained with the $\hat{H}^{2D,GE}$ Hamiltonian are exactly the same as those obtained with the 2D(ϕ_1, ϕ_2) model given in Table 2. Note that the basis functions defined by Equation (17) are eigenfunctions of the uncoupled system, thus they provide an efficient basis set for the expansion of the energy eigenstates of the weakly coupled system, considerably facilitating the determination of the K_{GE} labels provided in the third column of Table 2 for the 2D(ϕ, α_{GE}) model.

4.4. The 2D(ϕ, α_{BE}) BE rovibrational model

The second coordinate transformation employed within this section is specified as follows:

$$\begin{aligned} \phi &= \phi_2 - \phi_1, \\ \alpha_{BE} &= \frac{\phi_1 + \phi_2}{2}, \end{aligned} \tag{21}$$

with ϕ and α_{BE} describing vibrational and rotational dofs, respectively. The transformed Hamiltonian is

$$\begin{aligned} \hat{H}^{2D,BE} &= -b_{H_2}\left(2\frac{\partial^2}{\partial\phi^2} + \frac{1}{2}\frac{\partial^2}{\partial\alpha_{BE}^2}\right) + \hat{V}(\phi) \\ &= -b_{H_2}\left(2\frac{\partial^2}{\partial\phi^2} - \frac{1}{2}\hat{L}^2\right) + \hat{V}(\phi), \end{aligned} \tag{22}$$

where $\hat{L} = -i\frac{\partial}{\partial\alpha_{BE}}$. The form of $\hat{H}^{2D,BE}$ is in line with the matrix elements of $\mathbf{G}^{BE,4D}$ (see Equation (4)) and suggests that ϕ and α_{BE} are not coupled in this model. However, the coordinate transformation of the integrals giving Hamiltonian matrix elements shows that the integration limits of ϕ indeed depend on the actual value of α_{BE}:

$$\begin{aligned} \mathbf{H}^{2D}_{k_1,k_2;k_1',k_2'} &= \frac{1}{4\pi^2}\int_0^{2\pi} d\phi_1 \int_0^{2\pi} d\phi_2 \exp(-ik_1\phi_1)\exp(-ik_2\phi_2) \\ &\quad \times \hat{H}^{2D}\exp(ik_1'\phi_1)\exp(ik_2'\phi_2) \\ &= \frac{1}{4\pi^2}\Bigg[\int_0^{\pi} d\alpha_{BE}\int_{-2\alpha_{BE}}^{2\alpha_{BE}} d\phi \\ &\quad \times \exp(-i(k_1+k_2)\alpha_{BE})\exp\left(-i\frac{k_2-k_1}{2}\phi\right) \\ &\quad \times \hat{H}^{2D,BE}\exp(i(k_1'+k_2')\alpha_{BE})\exp\left(i\frac{k_2'-k_1'}{2}\phi\right) \\ &\quad + \int_{\pi}^{2\pi} d\alpha_{BE}\int_{2\alpha_{BE}-4\pi}^{4\pi-2\alpha_{BE}} d\phi \exp(-i(k_1+k_2)\alpha_{BE}) \\ &\quad \times \exp\left(-i\frac{k_2-k_1}{2}\phi\right) \\ &\quad \times \hat{H}^{2D,BE}\exp(i(k_1'+k_2')\alpha_{BE})\exp\left(i\frac{k_2'-k_1'}{2}\phi\right)\Bigg] \\ &= \delta_{LL'}\left[b_{H_2}\left(2K_{BE}^2 + \frac{1}{2}L^2\right)\delta_{K_{BE},K_{BE}'} + V_{K_{BE}-K_{BE}'}\right] \\ &= \mathbf{H}^{2D,BE}_{K_{BE},L;K_{BE}',L'}, \end{aligned} \tag{23}$$

where $K_{BE} = (k_2 - k_1)/2 = K_{GE} - L/2$, and the Hamiltonian, the basis functions, the integral volume element, and the integration limits have been transformed according to the coordinate transformation defined by Equation (21). The new basis functions can be expressed as

$$f^{BE}_{K_{BE},L}(\phi, \alpha_{BE}) = \frac{1}{2\pi}\exp(iK_{BE}\phi)\exp(iL\alpha_{BE}), \tag{24}$$

with integer L, and integer (for even L) or half-integer (for odd L) K_{BE} values. Thus, the period of $f^{BE}_{K_{BE},L}(\phi, \alpha_{BE})$ with respect to α_{BE} is always 2π, but the period for ϕ, depending on the parity of L, is either 2π (for even L) or 4π (for odd L). Note that it is possible and reasonable to have the range of ϕ be 0–4π for all values of L. In this case, the normalisation factor in Equation (24) has to be changed from $(2\pi)^{-1}$ to $(2\sqrt{2}\pi)^{-1}$. By employing the matrix elements provided by Equation (23), it is straightforward to obtain the energy levels corresponding to the 2D(ϕ, α_{BE}) BE rovibrational model. Alternatively, by performing similar manipulations to those carried out at the end of the previous subsection, one can show that ϕ-dependent periodic DVR basis functions can also be used. Energy levels obtained from the BE model agree with their 2D(ϕ, α_{GE}) GE and 2D(ϕ_1, ϕ_2) counterparts.

5. The Eckart and Sayvetz embeddings for H_5^+

In a recent study [18], some of us computed the rovibrational energy levels of H_5^+ variationally using the internal coordinates of Figure 1 and employing the geometric embedding. To supplement the unusual results obtained, *vide infra*, the Eckart embedding [41] was also applied in the hope that it reduced the coupling between the vibrational and rotational dofs.

In Ref. [18], the Eckart embedding resulted in energy levels which differed from the results obtained with geometric embedding and followed the rigid-rotor model. This led some of us [18] to question the applicability of the Eckart embedding in this particular case. Furthermore, a flexible Eckart embedding [42] (hereafter called Sayvetz embedding) was also introduced in Ref. [18], where the reference structure follows the torsional motion. The Sayvetz embedding resulted in energy levels which were in agreement with the ones computed using the geometric embedding. Here, we are clarifying a statement made about the Eckart embedding in Ref. [18].

The translational Eckart condition, $\sum_{\alpha=1}^{N} m_\alpha \mathbf{r}_\alpha = \mathbf{0}$, is satisfied automatically for H_5^+ with the current set of coordinates in any embedding if only torsional motions of the H_2 units are considered. This is due to the fact that with

$x = y = z = 0$, the COM of the molecule always lies at the origin of the body-fixed coordinate system (see Figure 1).

The case of the rotational Eckart condition, $\sum_{\alpha=1}^{N} m_\alpha(\mathbf{r}_\alpha \times \mathbf{a}_\alpha) = \mathbf{0}$, where $\mathbf{a}_\alpha$ denote the reference positions, is almost as straightforward. Using the nuclear position vectors of the bisector embedding (Equation (2)) and the D_{2d} structure of H_5^+ as the reference structure, the rotational Eckart conditions are satisfied. This leads to the conclusion that the bisector embedding is equivalent to the Eckart embedding for the models investigated. This also implies that using the Eckart embedding also requires the use of the manipulations explained for the 2D(ϕ, α_{BE}) BE rovibrational model (see the text below Equation (24)). However, in the geometric embedding, using the nuclear position vectors of Equation (3) and the same D_{2d} reference structure, the rotational Eckart condition is not satisfied. Nevertheless, it can be shown that with a reference structure which follows the torsional motion, the rotational Eckart condition is also satisfied. This indicates that the geometric embedding is equivalent to the Sayvetz embedding.

These findings suggest that a previous statement made by some of us [18] about the inadequateness of the Eckart embedding when used for H_5^+ was incorrect. As expected and shown here, an appropriate use of the Eckart embedding in the case of H_5^+ also results in correct rotational-vibrational energy levels.

6. On the rovibrational energy level structure of H_5^+ and its models

In a recent publication [18], some of us noted that the rovibrational energy levels of H_5^+ display several highly peculiar characteristics. Some of these unusual features are displayed by the $E(V \neq 0)$ results of Table 2. The 2D(ϕ, α_{GE}) and 2D(ϕ, α_{BE}) rovibrational models of H_5^+ can be interpreted such that the B and C rotational constants are zero and the $A = b_{H_2}/2$ rotational constant is about 26 cm^{-1}. Several important conclusions can be drawn from the computed results presented in Table 2.

First, consider the $V = 0$ states. All these states can be described by a single $|K_{GE}|$ value. Labelling of the four and eightfold degenerate states requires two $|K_{GE}|$ values characterising an equal number of eigenstates, the only exceptions being the $|K_{GE}| = |k_2| = |k_1|$ cases where a single $|K_{GE}|$ is sufficient. The 12-fold degenerate states require three or four $|K_{GE}|$ values for their labelling, depending on whether the $k_1^2 + k_2^2 = 2(k_1')^2$ or the $k_1^2 + k_2^2 = (k_1')^2 + (k_2')^2$ relation holds. For example, the 12 eigenstates at 1333.42 cm^{-1} correspond to the $3^2 + 4^2 = 0^2 + 5^2$ relation, while the 12-fold degenerate 2666.84 and 3466.90 cm^{-1} eigenstates (not shown in Table 2) correspond to $1^2 + 7^2 = 5^2 + 5^2$ and $4^2 + 7^2 = 1^2 + 8^2$, respectively.

Second, let us turn on the potential. This will affect the energy levels and the wavefunctions, and thus their labelling, in a number of ways. (1) For $V \neq 0$, $|K_{GE}|$ is no longer a good quantum number for the eigenstates corresponding to a given $|L|$. On the other hand, $|K_{BE}|$ appears to provide a unique set of labels for the energy levels corresponding to a given $|L|$, increasing $|K_{BE}|$ corresponds to increasing energy order. (2) The $L = 0$ energy values, which one could call vibrational band origins (VBOs), always change when the potential is turned on. The $L = 0$ energy values of Table 2 are in fact the same as the energies presented in Table 1 for the 1D(ϕ) model. (3) When considering *even* values of $|L| > 0$, the following can be observed: (a) The energy of the first level ($i = 1$ and $|K_{BE}| = 0$) appears to be independent of the height of the barrier in the potential, although the corresponding wave functions change as the PES changes. (b) While the energies do change in the previously ($V = 0$) four and eightfold degenerate $|K_{GE}| = |k_2| = |k_1|$ cases, one $|K_{GE}|$ is still sufficient to label the eigenstate. In all other cases, there is a 50–50 mixing of x and y basis states, which is indicated in the corresponding column of Table 2 employing the $(x - y)$ notation. (c) All the 'rovibrational' energy levels can be simply calculated via the equation $E(|L_{even}| \neq 0) = E(L = 0) + b_{H_2}L^2$, i.e., by knowing the 'vibrational' energies and the value of $|L|$, as suggested by the BE model (a similar statement holds for the wavefunctions, as well). For example, a constant splitting of 40.02 cm^{-1} is first observed for the first two purely torsional VBOs ($L = 0$, $i = 2$ and 3), and the same splitting is also found between the pairs of states with $i = 2$ and 3, $|K_{BE}| = 1$ and even $|L|$ values. (4) For *odd* values of $|L|$ similar but somewhat different statements hold: (a) In the previously ($V = 0$) fourfold degenerate cases, the fourfold degeneracy remains and the same $|K_{GE}|$ values can be used to label the eigenstates. (b) In the previously ($V = 0$) eightfold degenerate cases, there is a splitting into two fourfold clusters, where one $|K_{GE}|$ labels two eigenstates and another one the remaining two. Such cases are indicated in the corresponding column of Table 2 by employing the (x, y) notation. (c) For the previously ($V = 0$) 12-fold degenerate states, the two subcases discussed above for even and odd $|L|$ values will both be present. (d) All the 'rovibrational' energy levels can still be simply calculated based on the $|L| = 1$ energies and the value of $|L|$ via the equation $E(|L_{odd}| \neq 0) = E(L = 1) + b_{H_2}(L^2 - 1)$, as also suggested by the BE model.

Third, an unanticipated but seemingly general aspect of the rovibrational energy level structure of H_5^+ comes in the fact that energy states that are labelled as $|L| = 1$, $|K_{GE}| = 1$ (and which have energies of 52.72 cm^{-1}) are lower in energy than the $L = 0$, $|K_{GE}| = 1$ level (which is found at 88.06 cm^{-1}). This apparently odd energy ordering, where the $|L| = 1$ level is lower in energy than the corresponding $L = 0$ state, is related to the difference in the integration limits for ϕ when L is even or odd, as described above. When the range of ϕ is made to be [0,4π] in all cases, one finds that the nodal structure for the states with $L = 0$ and $|K_{GE}| = 1$ have two quanta in the torsion rather than

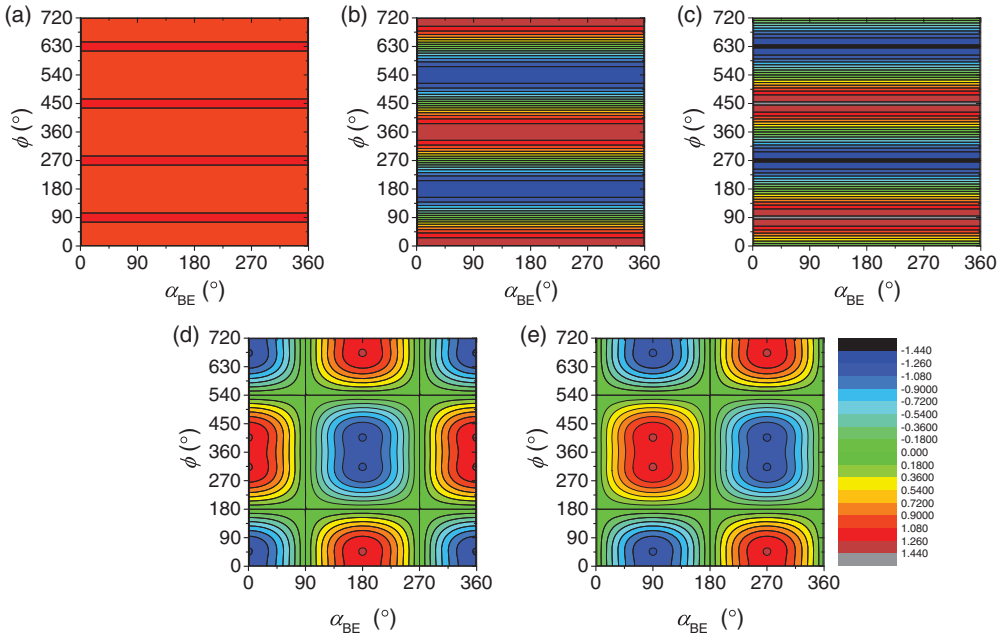

Figure 3. Plot of five wave functions obtained by solving the $\hat{H}^{2D,BE}$ model Hamiltonian with the potential defined in Equation (7); (a) provides the ground state ($L = K_{BE} = 0$ and consequently $k_1 = k_2 = 0$), (b) and (c) correspond to linear combinations of states with $L = 0$ and $|K_{BE}| = 1$ ($k_1 + k_2 = 0$ and $|k_1 - k_2| = 2$), while (d) and (e) show two linear combinations of states with $|L| = 1$ and $|K_{BE}| = 1/2$ ($|k_1 + k_2| = |k_1 - k_2| = 1$).

one, while the states with $|L| = 1$, $|K_{GE}| = 1$ have only one quantum in the torsion. If we focus on the L and $|K_{BE}|$ quantum numbers, the energy progressions appear to be more consistent with expectations (see Table 2). This change in the quantum number descriptions can also be seen in the wave functions for $|L| = 0$ and 1 with $|K_{BE}| \leq 1$, using the potential defined in Equation (7), plotted in Figure 3. As clearly seen, for the ground state (Figure 3(a)), the value of the wave function is essentially constant and the wave function is independent of α_{BE}. When $L = 0$ and $|K_{BE}| = 1$ ($|k_1| = |k_2| = 1$ and $k_1 + k_2 = 0$), the nodal pattern in ϕ is consistent with two quanta in the torsion, rather than one. In contrast, when $|k_1|$ and $|k_2|$ equal 1 and 0, there are half as many nodes in ϕ, and now there is a node in α_{BE} consistent with the assignment of this state to $|L| = 1$ and $|K_{BE}| = 1/2$. While this choice of coordinates and quantum numbers results in a more straightforward energy progression, it still leads to atypical behaviour as the requirement that both k_1 and k_2 take on integer values means that $|K_{BE}|$ can be either integer or half integer. The $E(V = 0)$ states provide a perfect physical explanation for this unusual characteristics of the energy level set.

Fourth, it is of general interest to ask how the computed rovibrational energies change as the torsional barrier changes. The results of this analysis are provided in Figure 4, where the energies and the value of V_0 in Equation (7) are provided in reduced units, i.e., scaled by the rotor constant for H_2, b_{H_2}. In this plot, the energies

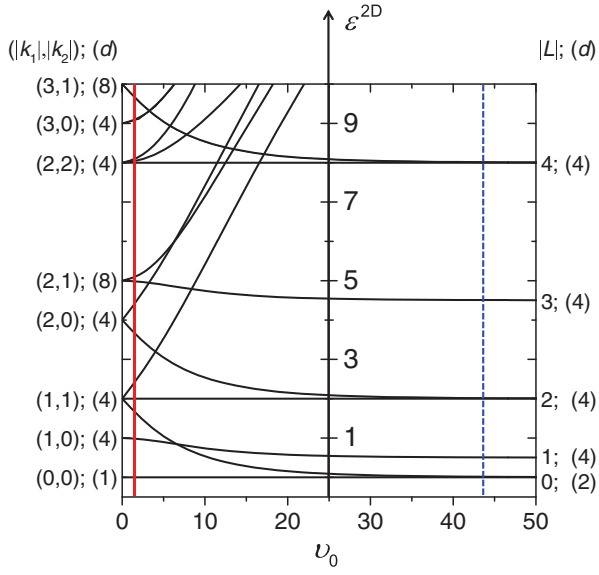

Figure 4. A plot showing the correlation between the energy levels for the $\hat{H}^{2D,BE}$ model of H_5^+ and the size of V_0 in Equation (7), via reduced energies and the reduced $\upsilon_0 = V_0/b_{H_2}$ quantity. In the limit of small υ_0, the eigenvalues are labelled by the absolute values of the quantum numbers for the uncoupled basis, ($|k_1|$, $|k_2|$), while in the large barrier limit, the energies are labelled by $|L|$. In addition, the degeneracy of the states are provided by (d). The vertical red and dashed blue lines represent the values of υ_0 for H_5^+ and methanol, respectively.

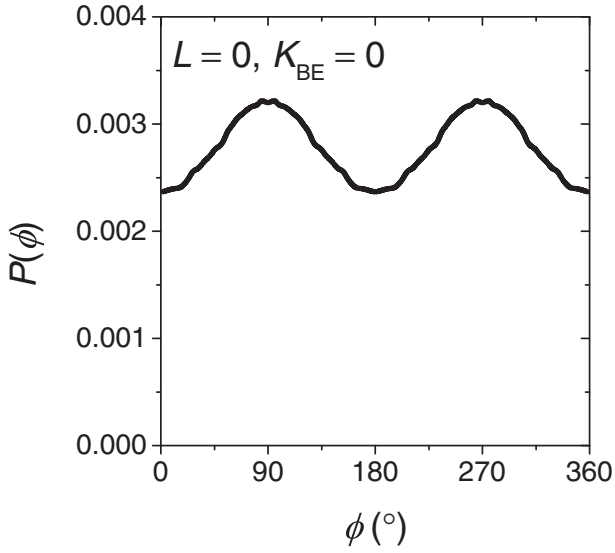

Figure 5. Plot of the projection of the diffusion Monte Carlo ground-state probability amplitude for H_5^+ [35] obtained using the potential of Aguado *et al.* [28].

$\varepsilon^{2D} = E^{2D}/b_{H_2}$ are reported relative to the zero-point energy and as a function of $\upsilon_0 = V_0/b_{H_2}$, where V_0 represents the height of the barrier in the torsion potential. The plotted eigenvalues are described in terms of the quantum numbers for the uncoupled basis, $|k_1|$ and $|k_2|$ (left) or their sum $|L| = |k_1 + k_2|$ (right), and correspond to the two limiting cases, i.e., the zero and the very large barrier cases, respectively. The degeneracy (d) of each level is also provided. As seen, in the limit of large υ_0, the tunneling structure expected for semirigid molecules is recovered, where the degeneracy reflects the double-well nature of the potential as well as the fact that the energy depends on $|L|$ and not its sign. In this plot, the value of υ_0 that is appropriate for H_5^+ is 1.5, and this is indicated with a red vertical line in the figure. As anticipated by the discussion above, this corresponds to an energy level progression that is very close to the barrierless ($\upsilon_0 = 0$) limit. The value of υ_0 that corresponds to the barrier in methanol is approximately 44 [43,44] and is shown with a blue dashed line in Figure 4. This value is reflected in the fact that the rovibrational energy level pattern in methanol is much closer to the high barrier limit than to the barrierless limit. Other molecules of note are dimethyl acetylene, which has a small value of $\upsilon_0 = 1.12$ [45], corresponding to a case very similar to H_5^+, and ethane, characterised by a very large value of $\upsilon_0 = 188$ [46,47]. In fact, as noted by Bunker and Jensen [48], 'except in ultrahigh resolution spectroscopic studies ethane can be considered to be a rigid molecule and the possibility of torsional tunneling can be neglected'. It is also of interest to note that for tolane (diphenyl-acetylene) $\upsilon_0 = 533$ [49].

Before concluding this section, it is of interest to consider how well these models are expected to describe the full-dimensional system in which all nine vibrational degrees of freedom are considered. As some of us reported in Ref. [18], the energy pattern obtained in the full-dimensional calculations reflects the results of the model systems described here. This is also consistent with the projections of the ground-state probability amplitude, evaluated using the potential surface of Aguado *et al.* [28,35], plotted in Figure 5. While the projected probability amplitude shows structure, the amplitude of the oscillation is much smaller than the average amplitude. This indicates that even when zero-point energy is included in all of the vibrational degrees of freedom, the internal rotor in H_5^+ remains nearly isotropic. Preliminary DMC results of rotation/torsion excited states of H_5^+ show energy level patterns similar to those described above.

7. Conclusions

The different 1D and 2D Hamiltonians, based on the ϕ torsional and α rotational coordinates, which can be considered as reduced-dimensional models describing internal motions of the H_5^+ molecular ion, derived as part of this work and employed in energy-level computations, yield the following important conclusions: (a) the same 1D(ϕ) vibrational model emerges from both the 2D(ϕ, α_{GE}) GE and 2D(ϕ, α_{BE}) BE models, where GE and BE refer to the geometric and bisector embeddings, respectively (see Figure 2); (b) equivalent 2D rovibrational models corresponding to different coordinates and embeddings provide the same energy levels, as required; (c) in case of the 2D(ϕ_1, ϕ_2) model of two torsional motions uncoupled in the kinetic energy operator, separation of the rovibrational levels according to the L angular momentum quantum number is not straightforward; (d) both the 2D(ϕ, α_{GE}) GE and 2D(ϕ, α_{BE}) BE models allow the separate computation of rovibrational levels with different L values; and (e) the 2D(ϕ, α_{GE}) GE and 2D(ϕ, α_{BE}) BE models provide correct energy levels and wavefunctions with either periodic complex exponential or exponential DVR basis functions. Furthermore, these modelling efforts provide a clear and simple physical interpretation of (a) some of the highly peculiar characteristics of the energy level structure of H_5^+ and (b) the differences in the rovibrational energy level patterns and the related degeneracies of H_5^+ and dimethyl acetylene, two molecules characteristic of the zero-barrier limit, as compared to methanol and ethane, two molecules corresponding to the large-barrier limit.

Acknowledgements

Z. Lin would like to acknowledge the Graduate School at The Ohio State University for a Presidential Fellowship.

Disclosure statement

No potential conflict of interest was reported by the authors.

Funding

The work described received support from the Scientific Research Fund of Hungary (OTKA) [grant number NK83583]; the US National Science Foundation [grant number CHE-1213347]; an ERA-Chemistry Grant.

References

[1] H.H. Nielsen, Rev. Mod. Phys. **23**, 90 (1951).
[2] I.M. Mills, in *Molecular Spectroscopy: Modern Research*, edited by K.N. Rao and C.W. Mathews (Academic Press, New York, 1972), Vol. 1, pp. 115–140.
[3] I.M. Mills, in *Specialist Periodical Reports, Theoretical Chemistry*, edited by R.N. Dixon (The Chemical Society, London, 1974), Vol. 1.
[4] D.A. Clabo, Jr, W.D. Allen, R.B. Remington, Y. Yamaguchi, and H.F. Schaefer III, Chem. Phys. **123**, 187 (1988).
[5] W.D. Allen, Y. Yamaguchi, A.G. Császár, D.A. Clabo, Jr, R.B. Remington, and H.F. Schaefer III, Chem. Phys. **145**, 427 (1990).
[6] E.B. Wilson, J.C. Decius, and P.C. Cross, *Molecular Vibrations* (McGraw-Hill, New York, 1955).
[7] S. Califano, *Vibrational States* (Wiley, London, 1976).
[8] H.W. Kroto, *Molecular Rotation Spectra* (Dover, New York, 1992).
[9] M.G. Bucknell and N.C. Handy, Mol. Phys. **28**, 777 (1974).
[10] R.J. Whitehead and N.C. Handy, J. Mol. Spectrosc. **55**, 536 (1975).
[11] S. Carter and N.C. Handy, J. Mol. Spectrosc. **95**, 9 (1982).
[12] S. Carter and N.C. Handy, Comp. Phys. Rep. **5**, 115 (1986).
[13] N.C. Handy, Int. Rev. Phys. Chem. **8**, 275 (1989).
[14] J.F. Gaw, A. Willetts, W.H. Green, and N.C. Handy, in *Advances in Molecular Vibrations and Collision Dynamics*, edited by J.M. Bowman (JAI Press, Greenwich, CT, 1990).
[15] N.C. Handy, Mol. Phys. **61**, 207 (1987).
[16] A.G. Császár and N.C. Handy, J. Chem. Phys. **102**, 3962 (1995).
[17] A.G. Császár and N.C. Handy, Mol. Phys. **86**, 959 (1995).
[18] C. Fábri, J. Sarka, and A.G. Császár, J. Chem. Phys. **140**, 051101 (2014).
[19] J.T. Hougen, I. Kleiner, and M. Godefroid, J. Mol. Spectrosc. **163**, 559 (1994).
[20] L.-H. Xu and J.T. Hougen, J. Mol. Spectrosc. **173**, 540 (1995).
[21] I. Kleiner and J.T. Hougen, J. Chem. Phys. **119**, 5505 (2003).
[22] I.M. Mills and H.W. Thompson, Proc. Roy. Soc. Lond. A **226**, 306 (1954).
[23] P.R. Bunker and H.C. Longuest-Higgins, Proc. Roy. Soc. Lond. A **280**, 340 (1964).
[24] G.M.P. Just, A.B. McCoy, and T.A. Miller, J. Chem. Phys. **127**, 044310 (2007).
[25] T. Pankewitz, A. Lagutschenkov, G. Niedner-Schatteburg, S.S. Xantheas, and Y.-T. Lee, J. Chem. Phys. **126**, 074307 (2007).
[26] M. Okumura, L.I. Yeh, and Y.-T. Lee, J. Chem. Phys. **88**, 79 (1988).
[27] Z. Xie, B.J. Braams, and J.M. Bowman, J. Chem. Phys. **122**, 224307 (2005).
[28] A. Aguado, P. Barragán, R. Prosmiti, G. Delgado-Barrio, P. Villarreal, and O. Roncero, J. Chem. Phys. **133**, 024306 (2010).
[29] T.C. Cheng, B. Bandyipadyay, Y. Wang, S. Carter, B.J. Braams, J.M. Bowman, and M.A. Duncan, J. Phys. Chem. Lett. **1**, 758 (2010).
[30] T.C. Cheng, L. Jiang, K.R. Asmis, Y. Wang, J.M. Bowman, A.M. Ricks, and M.A. Duncan, J. Phys. Chem. Lett. **3**, 3160 (2012).
[31] Z. Lin and A.B. McCoy, J. Phys. Chem. Lett. **3**, 3690 (2012).
[32] A. Valdes, R. Prosmiti, and G. Delgado-Barrio, J. Chem. Phys. **136**, 104302 (2012).
[33] H. Song, S.-Y. Lee, M. Yang, and Y. Lu, J. Chem. Phys. **138**, 124309 (2013).
[34] P.H. Acioli, Z. Xie, B.J. Braams, and J.M. Bowman, J. Chem. Phys. **128**, 104318 (2008).
[35] Z. Lin and A.B. McCoy, J. Phys. Chem. A **117**, 11725 (2013).
[36] E. Mátyus, G. Czakó, and A.G. Császár, J. Chem. Phys. **130**, 134112 (2009).
[37] C. Fábri, E. Mátyus, and A.G. Császár, J. Chem. Phys. **134**, 074105 (2011).
[38] C. Fábri, E. Mátyus, and A.G. Császár, Spectrochim. Acta A **119**, 84 (2014).
[39] Y. Yamaguchi, J.F. Gaw, R.B. Remington, and H.F. Schaefer III, J. Chem. Phys. **86**, 5072 (1987).
[40] C.C. Lin and J.D. Swalen, Rev. Mod. Phys. **31**, 841 (1959).
[41] C. Eckart, Phys. Rev. **47**, 552 (1935).
[42] A. Sayvetz, J. Chem. Phys. **7**, 383 (1939).
[43] Y.Y. Kwan and D.M. Dennison, J. Mol. Spectrosc. **43**, 291 (1972).
[44] E. Herbst, J.K. Messer, and F.C. DeLucia, J. Mol. Spectrosc. **108**, 42 (1984).
[45] C. di Lauro, P. R. Bunker, J.W.C. Johns, and A.R.W. McKellar, J. Mol. Spectrosc. **184**, 177 (1997).
[46] J.D. Kemp and K.S. Pitzer, J. Chem. Phys. **4**, 749 (1936).
[47] I. Nakagawa and T. Shimanouchi, J. Mol. Spectrosc. **39**, 255 (1971).
[48] P.R. Bunker and P. Jensen, *Molecular Symmetry and Spectroscopy*, 2nd ed. (NRC Research Press, Ottawa, 1998).
[49] D. Xu and A.L. Cooksy, J. Mol. Struct. THEOCHEM **815**, 119 (2007).